Sunlight Induces the Production of Atmospheric Volatile Organic Compounds (VOCs) from Thermokarst Ponds

Tao Wang, Carmen Kalalian, Daniel Fillion, Sébastien Perrier, Jianmin Chen, Florent Domine, Liwu Zhang, Christian George

Sunlight Induces the Production of Atmospheric Volatile Organic Compounds (VOCs) from Thermokarst Ponds

Tao Wang[1,2], Carmen Kalalian[1], Daniel Fillon[3,4,5], Sébastien Perrier[1], Jianmin Chen[2], Florent Domine[3,4,5], Liwu Zhang[2]*, Christian George[1]**

1 Univ Lyon, Université Claude Bernard Lyon 1, CNRS, IRCELYON, 69626, Villeurbanne, France

2 Shanghai Key Laboratory of Atmospheric Particle Pollution and Prevention, Department of Environmental Science & Engineering, Fudan University, Shanghai, 200433, China

3 Takuvik Joint International Laboratory, Université Laval (Canada) and CNRS-INSU (France), Québec, Canada

4 Centre d'Études Nordiques, Université Laval, Québec, Canada

5 Department of Chemistry, Université Laval, Québec, Canada

KEYWORDS: permafrost, thermokarst, volatile organic compounds (VOCs), Arctic, photochemistry

SYNOPSIS: Photoproduction of VOCs from thermokarst ponds water is not directly correlated to the amount of dissolved organic matter but rather to the availability of organic matters at the top layers of the liquid phase.

ABSTRACT: Ground subsidence caused by permafrost thaw causes the formation of thermokarst ponds, where organic compounds from eroding permafrost accumulate. We photolyzed water samples from two such ponds in Northern Quebec and discovered the emission of volatile organic compounds (VOCs) using mass spectrometry. One pond near peat-covered permafrost mounds was organic-rich, while the other near sandy mounds was organic-poor. Compounds up to C10 were detected, comprising O, N, and S atoms. The main compounds were methanol, acetaldehyde, and acetone. Hourly VOC fluxes under actinic fluxes similar to local solar fluxes might reach up to 1.7 nmol C m^{-2} s^{-1}. Unexpectedly, the fluxes of VOCs from the organic-poor pond were greater than those from the organic-rich pond. We suggest that different segregation of organics at the air/water interface may partly explain this observation. This study indicates that sunlit thermokarst ponds are a significant source of atmospheric VOCs, which may affect the environment and climate, via ozone and aerosol formation. Further work is required for understanding the relationship between pond organic composition and VOC emission fluxes.

INTRODUCTION

The top 3 m of terrestrial permafrost contains ~ 1000 Pg of carbon in the form of frozen vegetal debris that has accumulated over the past millennia[1,2]. This is significantly more than the atmospheric reservoir, 750 Pg[3], so that the mineralization of permafrost carbon induced by global warming has the potential to dramatically accelerate climate change. Projections of CO_2 and CH_4 emissions by thawing permafrost show a very wide range of values, most of which are between 7 and 100 Pg C by the year 2100 under the emission scenario RCP4.5[4-7]. However, these estimates are based on gradual permafrost thaw and ignore numerous processes, including rapid erosion and abrupt permafrost thaw[8], increased lightning and fires, and the rapid northward migration of trees[9]. Much greater emissions are therefore likely[8,10] and additional process studies are required for more reliable projections.

Many model parameterizations of the permafrost contribution to the atmospheric CO_2 budget rely on field or laboratory warming experiments that observe static processes[11,12]. Recent experiments however stress that lateral hydrological export could explain unexpectedly high losses of permafrost carbon[13]. Indeed, ice melting in permafrost leads to ground subsidence and geomorphological changes with the formation of erosion gullies and thermokarst ponds[14]. Erosion processes lead to the accumulation of dissolved and particulate organic carbon (DOC and POC) in thermokarst ponds[15,16], where it can be mineralized by microbial respiration and

photochemistry[17-19]. These latter processes are seldom included in models of permafrost carbon and in particular photolytic processes are ignored.

Photolysis of DOC and POC leads to the formation of CO_2 and its release to the atmosphere. However, products of incomplete oxidation are also formed and have been observed in the liquid phase[20-22]. The more volatile of these products can be released into the atmosphere and affect climate through several processes. The first one is their subsequent oxidation to CO_2. Since gaseous emission measurements from lakes focus on CO_2 and CH_4[19,23-25], neglecting this delayed CO_2 source may underestimate the greenhouse gas (GHG) emissions by lakes. Both field and laboratory studies indicate that incomplete photo-oxidation may represent up to half the photolysis products in lakes[22,26]. The second one is through the formation of ozone (O_3), a potent GHG[27], as many of the reactive organic compounds emitted are likely to have a strong O_3 formation potential[28]. Lastly, the further atmospheric oxidation of emitted compounds may lead to the formation of less volatile compounds that contribute to aerosol formation[29]. These aerosols affect climate through light scattering and cloud droplet formation[30,31].

Here we performed laboratory experiments to explore the release of volatile organic compounds (VOCs) from the photolysis of waters from thermokarst ponds in palsa and lithalsa environments. Palsas are peat-covered permafrost mounds whose collapse feeds large amounts of organic matter into thermokarst ponds. Lithalsas are also permafrost mounds, but without peat, and the amount and nature of organic matter released to

thermokarst ponds are therefore expected to be different. Investigating the contrasted environments informs us about the variability of VOC emissions from thermokarst ponds. Below we will demonstrate that both sampled ponds are photochemically active. We will focus our attention on the different behaviors, and we discuss some aspects of the mechanisms involved and their underlying atmospheric implications at the sampling period and sites. The aim of this study is to encourage follow-up investigations to cover a wider range of conditions and spatiotemporal coverage.

MATERIALS AND METHODS

Sample Collection. The water samples used in this study were sampled in September 2019 from two contrasted thermokarst ponds located within the Canadian subarctic region at Kuujjuarapik (55°13'11'' N, 77°42'52" W) and Umiujaq (56°33'31" N, 76°28'57" W), as shown in Figure 1.

The Kuujjuarapik pond was located at the base of a collapsing palsa, and its water was visibly colored. The Umiujaq pond was surrounded by collapsing lithalsas with sandy soil, with water less colored than that from the Kuujjuarapik pond. The vegetation near Umiujaq was mostly lichen (*Cladonia* sp., mostly *C. stellaris*) and dwarf birch (*Betula glandulosa*) as detailed by Gagnon et al.[32]. The soil organic content is low in this area, around 4 kg m^{-2}[32]. In the sporadic permafrost zone, i.e., where we collected the water samples, numerous palsas and lithalsas have formed[33], as carbon reservoirs[34].

To collect the liquid samples, amber glass containers, initially rinsed with concentrated HNO_3 and then several times with ultrapure water, were then prefilled

with ultrapure water (18.2 MΩ.cm) and emptied at each site, and then filled with pond water. The triplicate samples were taken from the top 10 cm of the ponds. Blanks were also collected by opening and closing a bottle filled with ultrapure water at each site. All samples were frozen after collection and kept frozen until the actual photochemical experiments. The water samples were used for experiments as received i.e., unfiltered.

All results given below are blank-corrected, where the signals arising from blanks were subtracted from those of actual experiments. The VOC production from blanks was always significantly lower than those from collected samples (see Figure S1).

Experimental Setup. The approach used here was similar to that in our previous studies[35,36]. Briefly, a water- and Pyrex-filtered Xenon arc lamp delivered light irradiation in the actinic region (i.e., at wavelengths longer than ~ 280 nm) to a cylindrical quartz cell (2 cm diameter and 10 cm length) half-filled with 6 mL of the unfrozen pond water sample (Figure S2). The headspace of this reactor was then continuously purged with purified air at a flow rate of 200 mL min^{-1}, and its content of VOCs can be monitored by mass spectrometry (see below). After an initial stabilization period, the lamp was switched on, simulating solar irradiation for 180 min. The temperature fluctuations of the reactor were small, i.e., within ± 2°C (Figure S3). The experimental temperature (~ 25°C) is comparable to the maximum air temperature during the warm seasons in northern Quebec[37]. All experiments were performed in triplicates.

Figure S4 gives the spectral profiles of experimental and natural irradiation. Here, irradiance is calculated for the wavelength range of 280 - 420 nm because only radiation therein initiates photochemistry, since shorter wavelength may cause photolysis, while the energy of longer wavelength is not sufficient to induce photochemical reactions. Laboratory works commonly used this wavelength range to infer the photochemical production and fluxes of VOCs[38-40]. The experimental irradiance was 8.0 mW cm^{-2} as previously set[41,42], with an actinic flux of 1.20×10^{16} photon cm^{-2} s^{-1}. The surface of irradiated water sample in this laboratory study was several orders of magnitude lower than in nature, which reduces the flux of products. In order to meet our detection limits, the experimental irradiance was set to be higher than the natural levels at the sampling sites, but it still compares to the midday conditions elsewhere and should thus be regarded as realistic on Earth[43,44].

Measurement of VOCs. The VOCs produced upon irradiation were monitored using a high-resolution proton transfer reaction time-of-flight mass spectrometer (HR-PTR-ToF-MS, 8000, Ionicon Analytic GmbH, Austria). This technique was previously described by Müller et al.[45] and uses H_3O^+ as a soft ionization agent. This MS continuously sampled 200 mL min^{-1} gas flow at the reactor's outlet through a heated silicon steel tube. Spectra were acquired with a time resolution of 10 s at a mass resolution of 4500 m/Δm.

A calibration standard (TO-14A Aromatic Mix, Restek Corporation, USA) containing 14 VOCs (100 ppb for each diluted in N_2) was utilized to calibrate and test

the instrument performance. The sensitivity of standard compounds ranged between 15 and 70 cps/ppb, depending on the actual mass. As it was not possible to calibrate the instruments for each compound detected, the protonation rate constant was assumed to be 2×10^{-9} cm^3 s^{-1}, and therefore the mean sensitivity was set to be 30 cps/ppb. The mass calibration was performed by internal standards: hydronium ion isotope ($H_3{}^{18}O^+$, m/z = 21.022) and protonated acetone ($C_3H_7O^+$, m/z = 59.049) as commonly selected. The PTR-MS viewer software (version 3.2.8) was used for the raw spectral analysis, mass calibration, peak fitting, and area extraction. The mixing ratios of VOCs were finally determined based on the existing protocols[46]. More details are provided in Supporting Information (Text S1).

Aqueous Phase Analysis. For the liquid analysis, the solution before and after the VOC photochemical measurements were filtered, in contrast to the actual experiments, by a 0.22 μm polytetrafluoroethylene (PTFE) membrane filter (Pall Corporation, USA). Each treated sample was analyzed using a Q-Exactive Hybrid Quadrupole-Orbitrap mass spectrometer (Thermo Scientific, USA) to characterize the liquid molecules included. In addition, each sample's pH, optical properties, and concentration of non-purgeable organic carbon (NPOC) were measured. More details are provided in Supporting Information (Text S2).

Data Processing. The detected molecules in both phases can be characterized by a variety of indices, including oxygen-to-carbon ratio (O/C), hydrogen-to-carbon ratio (H/C), ring and double-bound equivalence (RDBE), aromaticity equivalent (Xc),

carbon oxidation state (OSc), and modified aromaticity index (AI_{mod}). Kendrick mass defect (KMD) analysis was performed to identify an array of compounds containing similar repeated functional groups[47]. Compounds whose elemental compositions only differ by the number of subunits would possess the same KMD level and line up horizontally in the KMD plot[48]. In this study, two subunits (CH_2, COO) were considered as key to describe the observed photochemistry. The characterization approaches are detailed in Text S3.

Correlation analysis and principal component analysis (PCA) were applied to the temporal VOC concentration profiles during the second half of light exposure to gain more insights into the relevant chemistry. Independent samples t-test was used to compare the experimental results of two different samples, whereas paired samples t-test compared the scenarios of pre and post irradiation for a specific sample. The outcome can be characterized by the *p* value, which indicates significant discrepancy or variation, when lower than 0.05. The measurement results from mass spectrometers are reserved for at least two decimals.

Carbon Flux Calculation. Following our previous studies on the photochemistry and VOC production at the air/sea interface[38,39,41,49,50], we calculated the carbon flux associated with the emission of a given VOC normalized to the surface of water available under the simulated sunlight, denoted as SF_{VOCs} (nmol C m^{-2} s^{-1}), according to:

$$SF_{VOCs} = \sum_{i=1}^{m} \frac{L \times C_i \times N_i \times 10^{-3}}{V_T \times A} \quad (1)$$

where L is the flow rate of air (~ 3.33 mL s^{-1}), C_i is the concentration of VOC i (ppb), N_i is the number of carbon atoms in VOC i (dimensionless), V_T is the molar volume of gas at temperature T (24.4 L mol^{-1} at 24.3℃), A is the area of surface water exposed to air (17.85 × 10^{-4} m^2), m is the number of organic species produced over the interface (38 for Kuujjuarapik and 55 for Umiujaq).

Given that the irradiance (I) of the natural study site differs from the experimental setting, we estimated the natural VOC fluxes, denoted as NF_{VOCs} (nmol C m^{-2} s^{-1}), by using a linear relationship between the photoinduced VOC production and irradiance as previously reported in other cases[41-43], as shown by equation (2). This correction method facilitates the comparison between the VOC emission fluxes derived from the different laboratory experiments and/or in-field measurements.

$$NF_{VOCs} = SF_{VOCs-dark} + (SF_{VOCs-light} - SF_{VOCs-dark}) \times \frac{I_{natural}}{I_{experimental}} \quad (2)$$

where $SF_{VOCs\text{-}dark}$ and $SF_{VOCs\text{-}light}$ are respectively the carbon fluxes attributed to the VOCs emitted before and during irradiation, $I_{experimental}$ is the experimental irradiance (8.0 mW cm^{-2}), $I_{natural}$ is the natural irradiance. Hourly $I_{natural}$ during the warm season of 2019 (1st June - 30th September) was measured at a meteorological site near the Umiujaq sampling site[51,52]. Temporal variations of $I_{natural}$ are given in Figure S5. Solar irradiance at Kuujjuarapik is very similar to that at Umiujaq (see Figure S4), therefore we used the Umiujaq data for both sites. Because the experimental irradiance was 22.7 folds of the natural daily mean level, the 180 min of irradiation in the laboratory simulates ~ 3 days' photochemistry in the field. Similar photoinduced VOC production

was previously observed across other water samples under strong and weak irradiation in a smog chamber system[38], and therefore no irradiance threshold exists in such type of investigations. Applying equation 2 (as described above) aims only to underline some differences in the pattern of emitted VOCs at both sampling sites, without capturing the full environmental variability of this Arctic region.

Implication Evaluation. To estimate whether the photochemically produced VOCs could locally (i.e., at the sampling sites) affect the O_3 budget under a given NO_x concentration, O_3 formation potential, *OFP* (μg m^{-3}), was calculated according to[28]:

$$OFP = \sum_{j=1}^{n} [X]_j \times MIR_j \quad (3)$$

where $[X]_j$ is the concentration of VOC *j* (μg m^{-3}), MIR_j is the maximum incremental reactivity (MIR) coefficient of VOC *j*, *n* is the number of VOC with documented *MIR* (22 for Kuujjuarapik and 33 for Umiujaq). *MIR* can be taken from the updated research results (https://intra.engr.ucr.edu/~carter/SAPRC/, last access: 10th, November 2022).

The calculated OFP can be normalized by the available air/water interfacial area to the simulated efflux of O_3, denoted as SF_{O3} (nmol m^{-2} s^{-1}), which is further corrected by the outdoor irradiance as that done for carbon flux to the natural F_{O3}, denoted as NF_{O3} (nmol m^{-2} s^{-1}), according to:

$$SF_{O_3} = \frac{L \times OFP \times 10^{-3}}{M_{O_3} \times A} \quad (4)$$

$$NF_{O_3} = SF_{O_3} \times \frac{I_{natural}}{I_{experimental}} \quad (5)$$

where M_{O3} is the molar mass of O_3 (48.0 g mol^{-1}).

RESULTS

As soon as the pond water was illuminated in the actinic region, a strong net photochemical production of a variety of VOCs can be observed (Figure 2a). The production is sustained and increasing, demonstrating that products are building up as long as the light was presented. Such production stopped when the light was switched off, with the concentration decreasing over time. While Figure 2a shows the integrated signal over all VOCs, more product details are presented in Table S1. The non-monotonic increases suggest that 2nd generation products are formed in both the liquid and gas phases. The net concentrations of total VOCs produced by photochemistry, determined by subtracting the background signal of each VOC (i.e., the averaged dark level before irradiation) by the corresponding maximum signal observed during the 180 min of irradiation, are 13.83 ± 2.01 ppb (mean ± standard error [SE]) and 20.14 ± 1.93 ppb for the samples from Kuujjuarapik and Umiujaq, contributed by 38 and 55 species, respectively. That is, the Umiujaq water exceeds the Kuujjuarapik water in the VOC photoproduction ($p < 0.05$, Figure S6). Thirty volatile products are common to both sites (Figure 2b).

Half of the VOCs emitted from the sunlit Kuujjuarapik sample contain ≤ 3 carbons, and these compounds are responsible for ~ 87% of the concentration of the Kuujjuarapik VOCs (Figure 2c, top half). By contrast, for the Umiujaq VOCs, while the total concentration is mainly contributed by C1-C3 species, most compounds contain ≥ 4 carbons. The concentration-weighted mean molecular mass of the Umiujaq

243 VOCs (53.26) is slightly greater than that of the Kuujjuarapik VOCs (50.98).
244 Furthermore, the VOCs are classified into CHO, CH, CHON, CHN, and CHS
245 subgroups according to their elemental compositions (Figure 2c, bottom half). The
246 CHO subgroup generally dominates the structure of VOCs observed, and the water
247 sample from Umiujaq is more efficient than that from Kuujjuarapik in producing all
248 these subgroups, except for the concentration of CHON and the number of CHS. The
249 average molecular formulas can be given as $C_{2.370}H_{4.839}O_{1.026}N_{0.064}S_{0.011}$ for the
250 Kuujjuarapik VOCs and $C_{2.651}H_{5.189}O_{0.948}N_{0.065}S_{0.003}$ for the Umiujaq VOCs.
251 Speciation of the observed photoproduced VOCs is given in Figure 2d. As the most
252 abundant product from the sunlit Kuujjuarapik pond surface water, CH_4O accounts for
253 28.3% of the total VOC concentration, followed by C_2H_4O (20.8%), C_3H_6O (16.1%),
254 C_3H_4O (4.6%), C_2H_2O (3.2%), $C_2H_4O_2$ (2.2%), CH_3NO (2.2%), C_4H_8O (2.1%), C_4H_6O
255 (1.4%), C_2H_5NO (1.3%) and other 28 compounds (accounting up to 17.8%). For the
256 pond water from Umiujaq, the ten most abundant compounds are C_2H_4O (30.9%),
257 CH_4O (15.5%), C_3H_6O (14.8%), C_3H_4O (5.0%), $C_2H_4O_2$ (2.4%), C_4H_8O (2.2%), C_3H_5N
258 (2.0%), C_2H_2O (2.0%), C_2H_6O (1.8%), C_4H_8 (1.7%), followed by the other 45 products
259 (accounting up to 21.8%). Also, for a given VOC, its relative production is negatively
260 correlated with its molecular weight (Figure S7).
261 Overall, three dominant species, CH_4O, C_2H_4O, and C_3H_6O that were normally
262 identified as methanol, acetaldehyde, and acetone (or possibly propanal or methyl vinyl
263 ether), are responsible for > 60% of the total VOC concentrations for both samples. A

statistical treatment (PCA in Figure S8) further reveals that these three compounds are not correlated and do originate from distinct processes, depending on the type of thermokarst pond surface water. Furthermore, positive correlations are common for the Umiujaq VOCs, whereas more negative correlations are observed among the Kuujjuarapik VOCs (Figure S9). In general, the Kuujjuarapik VOCs are more oxygenated, unsaturated, and aromatic than the Umiujaq ones, as reflected by the higher O/C and OSc, lower H/C and higher RDBE, and higher Xc and AI_{mod}, respectively (Table S2). Such molecular differences are certainly associated with the compositions of permafrost organic carbon in the two contrasted ponds studied here.

The photochemistry of both samples also differs significantly in the filtered liquid phase. The NPOC levels were 1320 ± 16 and 1070 ± 28 μM for the waters from Kuujjuarapik and Umiujaq, respectively, before irradiation. After irradiation, as shown in Figure S10, the NPOC level for Kuujjuarapik significantly increased to 1823 ± 170 μM ($p < 0.05$), whereas that of Umiujaq generally showed no significant change, with a value of 1003 ± 123 μM ($p > 0.05$). Moreover, as shown in Figure S11, the pH increased from 6.9 ± 0.0 to 7.4 ± 0.1 for the Umiujaq water ($p < 0.05$), while it decreased from 7.1 ± 0.0 to 6.9 ± 0.0 for the Kuujjuarapik water ($p < 0.05$). Lastly, the Umiujaq sample was observed to photobleach with irradiation, while for Kuujjuarapik the absorbance increased over time for wavelengths below 300 nm (Figure S12).

Our observations indicate that the organics contained in the thermokarst ponds are photochemically active and produce a variety of VOCs. Based on equation (1), under

285 the experimental setting, the integrated SF_{VOCs} for the Kuujjuarapik and Umiujaq ponds
286 are 2.83 and 4.61 nmol C m^{-2} s^{-1}, respectively. We further estimated the associated
287 NF_{VOCs} according to equation (2), and compared the two surface waters. The diel cycle
288 of hourly NF_{VOCs} is shown in Figure 3a, and both surface waters produced the highest
289 carbon fluxes at noon. The average NF_{VOCs} of the sampling day is estimated to be 0.21
290 nmol C m^{-2} s^{-1} across the Kuujjuarapik pond and 0.51 nmol C m^{-2} s^{-1} across the Umiujaq
291 pond. The photoinduced carbon flux across Kuujjuarapik pond primarily consists of
292 C_3H_6O (20.3%), C_2H_4O (17.5%), and CH_4O (12.0%), and that across Umiujaq pond is
293 mostly made of C_2H_4O (23.4%), C_3H_6O (16.7%), and CH_4O (5.8%), as shown by
294 Figure 3b. That is, acetaldehyde, acetone (or possibly propanal or methyl vinyl ether)
295 and methanol, which account for > 60% of the concentration of photoproduced VOCs
296 (see Figure 2d), also explain nearly half of the photoinduced VOC-associated carbon
297 flux over sunlit thermokarst ponds.
298 In order to further reveal the potential importance of the discovered photochemistry,
299 we speculate that the photoinduced VOC production for a longer time scale can be
300 estimated by extrapolating the measurement results to the natural irradiance of the warm
301 season (Figure S13). The highest daily NF_{VOCs} over the thermokarst ponds would occur
302 around the summer solstice. As irradiance decreased since then, the NF_{VOCs} over both
303 ponds generally decreased. Since NF_{VOCs} is influenced by temperature, irradiance, and
304 the properties of water, the atmospheric relevance of this photochemistry should be
305 accurately evaluated according to the actual situation.

DISCUSSION

To the best of our knowledge, this is the first detection and quantification of photochemically produced non-methane VOCs from thermokarst ponds. The weak VOC emissions before irradiation are probably explained by the diffusion to the gas phase of volatile species photoproduced under natural conditions before sampling. This is supported by the positive correlation between the individual VOC concentrations before and during irradiation (Figure S14). Thermokarst ponds are therefore a photochemical reactor that is able to transform permafrost carbon into atmospheric VOCs. VOCs have been reported to be also emitted directly by thawing permafrost, without the intervention of liquid phase photochemistry[53-55]. Current understanding is that these VOCs were produced by microbial metabolism, mostly anaerobic, and accumulated over the years before being released by thawing[53-55]. Here, however, we observed rapid VOC emission which is well correlated to irradiation conditions, so that production can be ascribed to photochemistry with reasonable certainty, rather than microbial production. This is in line with the observation of photoproducts over the liquid phase by others[43]. Given that many photoinduced reactions at the air/water interface are significantly enhanced in comparison to the corresponding gas- or liquid-phase bulk processes[56], and that our experiments were performed in the absence of any gaseous oxidants (and over very short residence time of the gas phase), the observed photochemical production of VOCs is mainly related to processes occurring at the air/water interface, with a possible contribution of aqueous bulk photochemistry.

Figure 4 illustrates the generic mechanism summarizing the photochemical production of VOCs from the surface water in these ponds. Thawing permafrost releases soil carbon into thermokarst ponds as POC and DOC, which both undergo an array of photochemical reaction pathways producing secondary DOC (DOCs), followed by the release of reacted DOC (DOCr) into the atmosphere as VOCs. Depending on the actual chemistry taking place, partial oxidation or decarboxylation leads to the formation of DOCr, which is more volatile and therefore more easily diffuses to the gas phase[20,22,57]. Given that the DOC loading of the Kuujjuarapik pond water significantly increased after irradiation, photolysis of POC to DOC may be responsible for the photochemistry in this palsa-affected surface water. In contrast, the decrease in absorbance of the Umiujaq water after irradiation indicates a decrease in photoreactive compounds, implying a lower transformation of POC to DOC.

Interestingly, the Kuujjuarapik pond water, which is organic-rich because it is affected by peat, is less efficient in the photochemical production of VOCs than the Umiujaq one which is organic-poor. Based on our previous research on the photochemistry of humic acids in multiphase systems similar to the one explored here[38,41], we are considering that the photoproduction observed for the thermokarst pond surface water is strongly impacted by the processes occurring at the air/water interface, and in particular by the availability of organic matters at the top layers of the liquid phase. In other words, if more appropriate precursors and oxidants are located at the sunlit air/water interface, more VOCs should be produced. Such availability is

highly pH-dependent, as for example more long-chain organic acids are increasingly soluble with increasing pH. Herein, the photo-decreased pH of the Kuujjuarapik water indicates the generation of organic acids derived from the photolysis of POC, during which the availability of surface acids decreases, whereas the photo-increased pH of the Umiujaq water implies the higher VOC production efficiency relying on photo-decarboxylation that can be described as the breakdown of carboxylic acids (R-COOH) to hydrocarbons (R-H) and CO_2 by sunlight[20,58]:

$$R - COOH \xrightarrow{hv} R - H + CO_2 \quad (6)$$

Another indication can be found in the evolution of the optical property of surface water. The photobleaching of the Umiujaq water implies that large compounds may photodegrade into smaller fragments with increased volatility. By contrast, the photo-enhanced absorbance of the Kuujjuarapik water indicates that photochemistry induces the increase of chemical functionalities, as evidenced by the photo-increased liquid aromaticity (Table S3). This variation may be attributed to the significant photolysis of POC, followed by the conversion of non-condensed aromatics to monoaromatics with higher AI_{mod}[59]. Overall, the photo-productivity of thermokarst pond water may thus be better predicted by considering the segregation and processes at the air/water interface than bulk organic concentration. This is in line with previous research in other aqueous systems, where the prevalence of interface processes was demonstrated[38,41].

As additionally suggested by the KMD plots for CH_2 (Figure S15) and COO (Figure S16), most photo-enhanced VOCs would "theoretically" form after the removal of one

369 or more target subunits (e.g., CH_2 or COO) from the photodegraded liquid compounds.
370 As an example, for both samples, $C_4H_4O_2$ may generate via the photo-dealkylation of
371 $C_5H_6O_2$ and its homologous series, and the photo-decarboxylation of $C_4H_6O_3$ or
372 $C_5H_6O_5$ would produce C_3H_6O. More suggested "precursor-product" pairs are listed
373 alongside the KMD plots in the Supporting Information. This points to the fact that, as
374 expected, we do observe multigeneration products from permafrost carbon conversion,
375 in agreement with the time profiles seen in Figure 2a. In comparison with the
376 Kuujjuarapik DOC, the Umiujaq DOC favors the photochemical production of VOCs
377 via decarboxylation channels. The efficient carboxyl loss follows the photo-increased
378 pH of the Umiujaq water and may be associated with more significant release of CO_2.
379 The relevant mechanisms may be much more complex than expected[60], depending on
380 the actual composition of the liquid phase.
381 Uncertainties may exist when reproducing the natural conditions. Firstly, the
382 production and release of volatile species are obviously changing with temperature[61,62].
383 Secondly, the carbons in thermokarst ponds are refreshed because (i) the permafrost is
384 always thawing by warming[14,63], rainfall[64], and wildfire[9]; (ii) wind above the shallow
385 pond will mix its liquid phase, including the vertical transport from deeper layers to
386 interface[65]; and (iii) the headwater streams feed the thermokarst ponds by bringing in
387 soil materials, especially during rain episodes[57,65]. The refresh of thermokarst pond
388 water will further change its physical properties (e.g., surface tension, liquid viscosity)
389 that are associated with the performance of air/water interface. Third and perhaps most

important, the "chemical history" (e.g., number of diurnal cycles) of permafrost carbons will also alter the liquid properties[20,22,26], followed by the variation of sunlight intensity at various depths and at the aqueous interface[57]. Those effects are certainly to be taken into account for the following studies.

IMPLICATIONS

It is worthwhile to mention that, the measurements performed by this study are too limited in space and time to provide a robust assessment of the VOC emission over the numerous thermokarst landscapes (3.6×10^6 km^2, ~ 20% of the northern permafrost region[14]), but given the vast area of this continuously formed natural air/water interface and the considerable emission fluxes of VOCs under sunlight, there is an urgent need to take throughout research of this photochemistry over the thermokarst ponds/lakes on Earth. Besides, temporal difference caused by the variations of carbon compositions, temperature, and irradiance are warranted in future works, as an attempt to reveal more characteristics of the photochemistry over thermokarst landscapes.

Nevertheless, the photochemical production of atmospheric VOCs may strongly impact the local air composition by generating significant airborne O_3 in the presence of NO_x. Simply based on equations (3) and (4), the SF_{O3} is calculated to be 3.83 nmol m^{-2} s^{-1} for the Kuujjuarapik sample and 7.34 nmol m^{-2} s^{-1} for the Umiujaq sample, under the experimental irradiance. Such results are much higher than the SF_{O3} over an authentic air/sea surface (0.51 nmol m^{-2} s^{-1}) investigated under the same experimental condition[42], suggesting that the photochemistry we discovered might present

411 considerable impacts on the local ozone budget. Corrected by equation (5), the daily
412 average NF_{O3} is 0.17 nmol m^{-2} s^{-1} for Kuujjuarapik and 0.32 nmol m^{-2} s^{-1} for Umiujaq,
413 during the entire warm season. The speciated contribution to O_3 formation is shown in
414 Figure S17. Among the Kuujjuarapik VOCs, C_2H_4O (acetaldehyde) is the largest O_3
415 contributor and accounts for 35.7% of the NF_{O3}, followed by C_3H_4O (acrolein, 11.4%),
416 $C_3H_4O_2$ (acrylic acid, 5.9%), $C_4H_6O_2$ (methyl acrylate, 5.5%), and C_4H_6O (methyl vinyl
417 ketone, 5.5%). In contrast, the main O_3 contributors among the Umiujaq VOCs are
418 C_2H_4O (acetaldehyde, 40.5%), C_3H_4O (acrolein, 9.4%), C_4H_8O (butanal, 4.4%), C_4H_8
419 (butene, 4.2%), and C_4H_6O (methyl vinyl ketone, 4.0%). The ranking of NF_{O3} differs
420 from that of VOC concentrations, implying that the atmospheric impact of this
421 photochemistry may not be directly determined by the magnitude of VOC emission. In
422 addition to altering locally the O_3 budget, the emissions of VOCs could also lead to an
423 increase in secondary organic aerosol formation, similar to what has been observed for
424 processes involving chromophoric materials at the air/sea interface[66]. This however
425 needs to be verified by further measurements.

426 Even though the VOC flux data were not reported for typical thermokarst landscapes,
427 a shallow post-glacial subarctic lake was recently explored for its in-field emission of
428 six non-methane VOCs[67], and the comparison results are listed in Table S4. At the end
429 of subarctic warm season (i.e., September), the lake presented net deposition fluxes of
430 methanol, acetaldehyde, acetone, and dimethyl sulfide, in contrast to the net emission
431 fluxes of isoprene and monoterpenes, eventually causing a net deposition flux of total

VOCs (-0.287 nmol C m^{-2} s^{-1}). The negative flux measured for the lake demonstrates that processes other than photochemistry were involved. In this study, both thermokarst pond waters owned more significant fluxes of methanol, acetaldehyde, and acetone than other three VOCs, corresponding to the photoinduced VOC emission fluxes of 0.080 and 0.172 nmol C m^{-2} s^{-1} for Kuujjuarapik and Umiujaq, respectively. While in nature it is difficult to isolate the contribution of photochemical processes to VOC emissions, the comparable absolute VOC fluxes obtained in the field and laboratory imply that the photochemistry reported here may have considerable implications for the budget and composition of atmospheric VOCs over subarctic water bodies.

Another obvious extension of this work is the comparison of the carbon fluxes of VOCs, which are currently not in-field measured over thermokarst ponds, with those of CH_4 and CO_2, which have been frequently measured over water bodies in the Arctic. The CO_2 and CH_4 fluxes have been measured above ponds close to those we sampled[19,68]. The average fluxes of CO_2 and CH_4 were respectively 143.84 and 5.80 nmol C m^{-2} s^{-1} over a lithalsa-affected thermokarst lake, and 676.28 and 40.60 nmol C m^{-2} s^{-1} over a palsa-affected thermokarst lake. In comparison, the VOC fluxes we measured are lower by 1-3 orders of magnitude. However, measurement conditions are not comparable. Our experiments were performed over samples with a maximal depth of ~ 0.55 cm, in contrast to the water bodies with depths of typically 2.0 m over which the gaseous CO_2 and CH_4 were produced. Furthermore, one study on a thermokarst lake near Kuujjuarapik[26] concluded that "only half of the light-associated DOC losses were

converted into CO_2", so that the fraction of VOCs produced by pond water photolysis may actually be significant. Meaningful comparisons would require operating under similar conditions for CO_2, CH_4 and VOC measurements. This is an analytical challenge, left for future research.

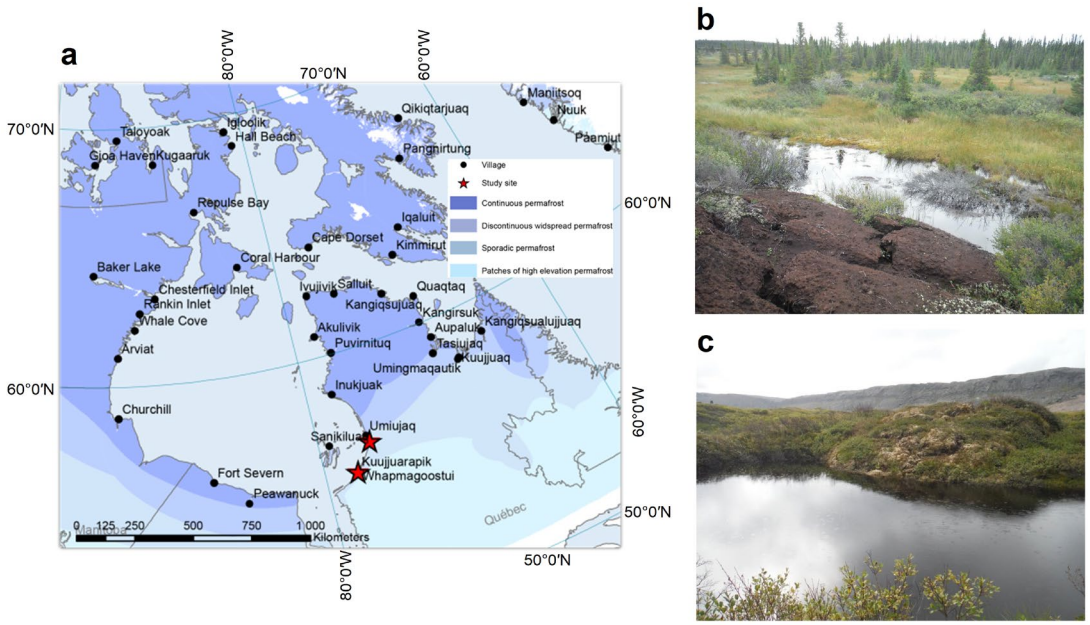

Figure 1. Overview of the studied thermokarst ponds.

(a) Geographical location of the sampling sites in Northern Quebec, Canada. The color scale distinguishes the type of permafrost. The study sites are located at the sporadic permafrost zone. Surrounding of the thermokarst ponds located at the **(b)** Kuujjuarapik and **(c)** Umiujaq sites.

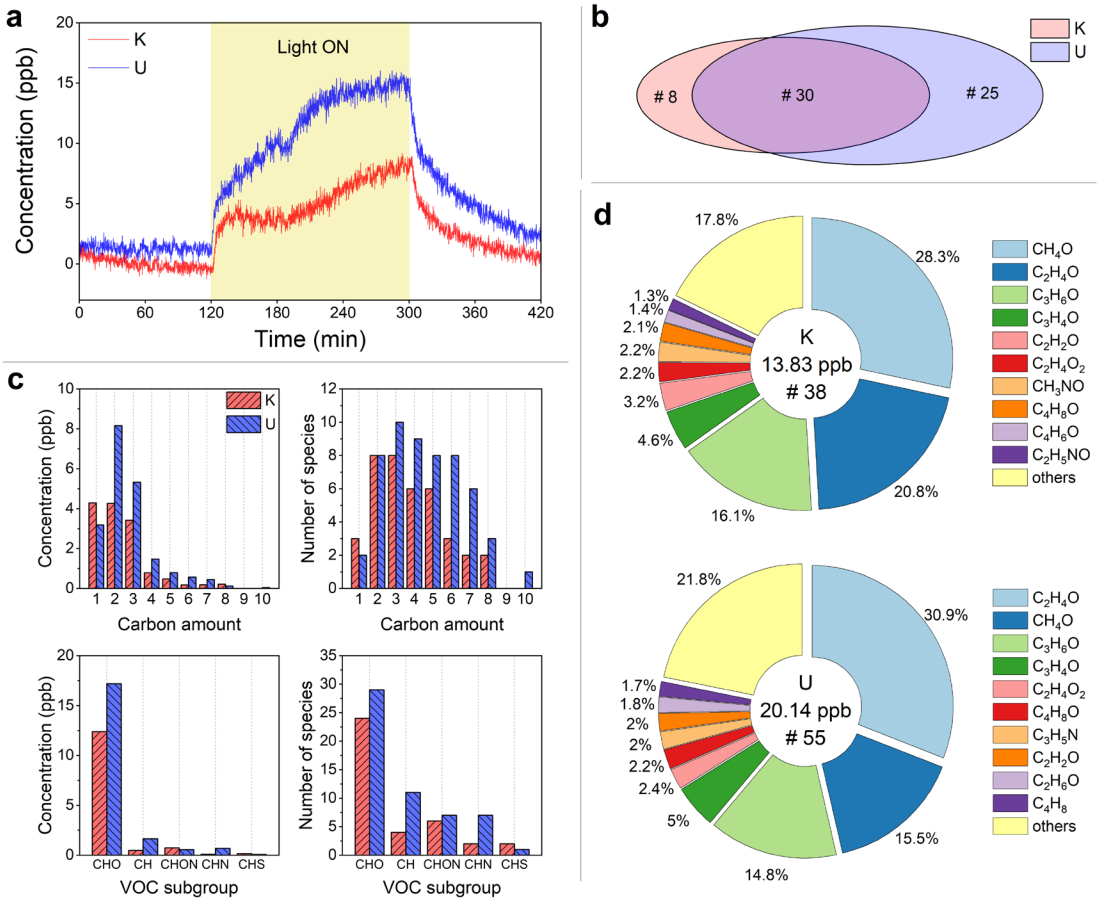

Figure 2. Characterization of the photoproduction of VOCs.

(a) Temporal profile of the concentration of VOCs produced from thermokarst pond water. Irradiation is highlighted by the yellow shading. The surface water samples were collected at the Kuujjuarapik (denoted as K) and Umiujaq (denoted as U) sites located in Northern Quebec, Canada. **(b)** Venn diagram for the numbers of VOCs photoemitted from the different samples. **(c)** Concentration or number of the photoproduced organic vapors as a function of carbon amount or VOC subgroup, varying with the type of thermokarst pond water sample. **(d)** Concentration proportions of the photoinduced VOCs. The ten most abundant species are listed for each sample. In total, 38 and 55 photoinduced VOCs, accounting for the measured volume concentrations of 13.83 and 20.14 ppb, were observed for the K and U samples, respectively.

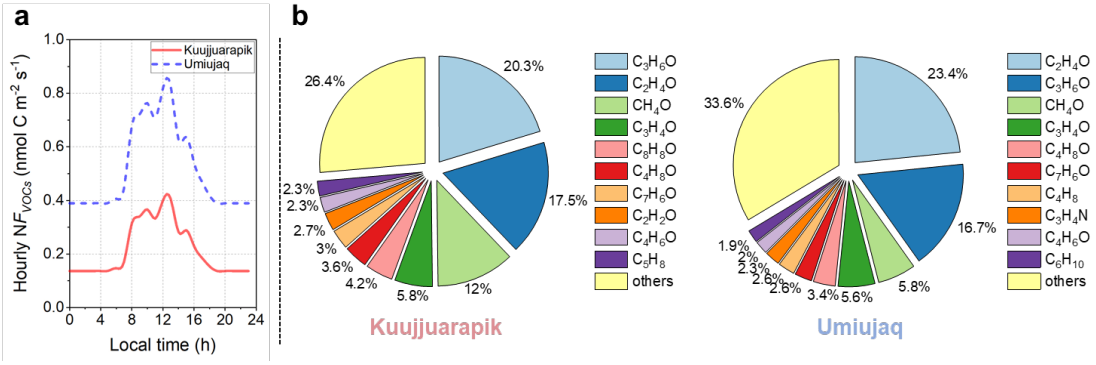

Figure 3. Evaluation of the photoproduction of VOCs.

(a) Diurnal variation of hourly natural VOC fluxes (NF_{VOCs}) over the studied thermokarst ponds. The emission flux of VOC-associated carbon can be calculated by equation (1) and further corrected by equation (2). The radiation data were recorded by a meteorological station near the Umiujaq pond during the sampling day: 4th September 2019.

(b) Contribution proportions of the photoinduced VOC-associated carbon fluxes (unit: nmol m^{-2} s^{-1}) over different thermokarst ponds. The ten most abundant species are listed for each site.

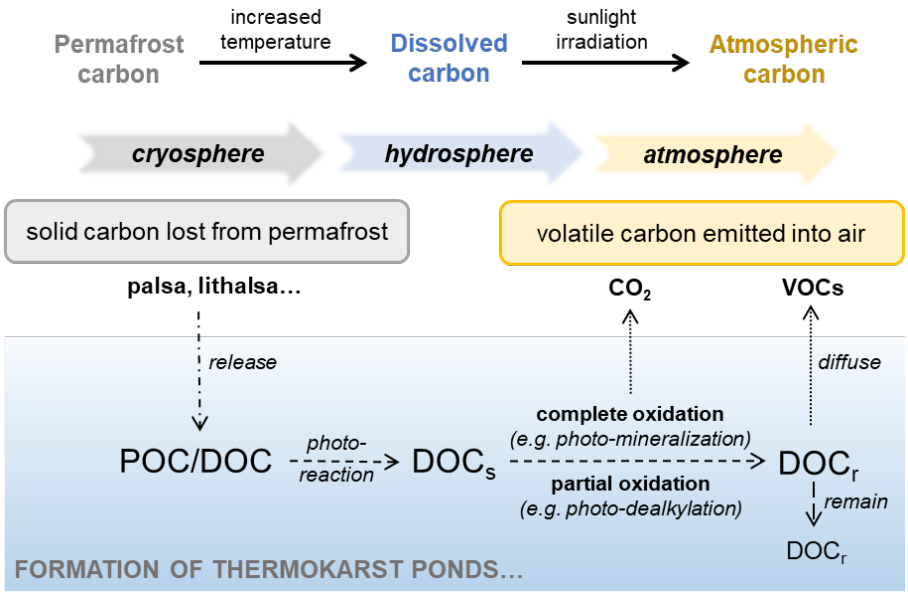

Figure 4. Schematic diagram for the photoinduced VOC production.

The photochemical production of VOCs can be briefly described as the evolution of soil carbon lost from thawing permafrost to dissolved carbon in thermokarst pond along with the increased temperature, followed by the photo-generation of volatile atmospheric carbon in surface water (solid line arrows). Overall, this photochemistry connects the Earth's cryospheric carbon reservoir to the atmosphere, via the hydrosphere. In detail, it comprises the release of permafrost carbon into thermokarst ponds (dash-dot line arrow), the photo-reaction of particulate organic carbon (POC) and dissolved organic carbon (DOC) in the liquid phase (short-dash line arrow), the further conversion of secondary DOC (DOCs) acting as VOC precursors (short-dash line arrow), the diffusion of volatile reacted DOC (DOCr) into the atmosphere as VOCs (dot line arrow), as well as the retention of DOCr in the liquid phase (dash line arrow). DOCs can also be completely oxidized to CO_2.

ASSOCIATED CONTENT

Supporting Information. Description of experimental procedures, methods of data analysis, characteristics (irradiance and actinic flux) of the experimental and natural irradiation; detailed information and molecular characterization of the detected VOCs, photoinduced evolutions of liquid phase, calculation of ozone formation potentials.

AUTHOR INFORMATION

Corresponding Author

Liwu Zhang（zhanglw@fudan.edu.cn）

Florent Domine (florent.domine@gmail.com)

Christian George (christian.george@ircelyon.univ-lyon1.fr)

Author Contributions

T.W., F.D., S.P., and C.G. designed research; T.W., C.K., and S.P. performed research; T.W., C.K., S.P., and C.G. analyzed the data; T.W., D.F., F.D., L.Z., J.C., S.P., and C.G. wrote the paper.

Notes

The authors declare no competing interest.

ACKNOWLEDGMENTS

The authors thank Letizia Abis, Xinke Wang, Sophie Tomaz, and Dandan Li (CNRS, IRCELYON) for their help in data analysis. F.D. and D.F. were funded by the French Polar Institute (IPEV, grant 1042) and NSERC discovery grant program. T.W. acknowledges the

National Natural Science Foundation of China (42205099) and the China Postdoctoral Science Foundation (2021M700792). L.W.Z. acknowledges the National Natural Science Foundation of China (22176036, 21976030, 22006020).

References

(1) Mishra, U.; Hugelius, G.; Shelef, E.; Yang, Y.; Strauss, J.; Lupachev, A.; Harden, J. W.; Jastrow, J. D.; Ping, C.; Riley, W. J.; Schuur, E. A. G.; Matamala, R.; Siewert, M.; Nave, L. E.; Koven, C. D.; Fuchs, M.; Palmtag, J.; Kuhry, P.; Treat, C. C.; Zubrzycki, S.; Hoffman, F. M.; Elberling, B.; Camill, P.; Veremeeva, A.; Orr, A. Spatial heterogeneity and environmental predictors of permafrost region soil organic carbon stocks. *Sci. Adv.* **2021**, *7*(9), eaaz5236.

(2) Palmtag, J.; Obu, J.; Kuhry, P.; Richter, A.; Siewert, M. B.; Weiss, N.; Westermann, S.; Hugelius, G. A high spatial resolution soil carbon and nitrogen dataset for the northern permafrost region based on circumpolar land cover upscaling. *Earth Syst. Sci. Data* **2022**, *14*(9), 4095-4110.

(3) IPCC, Climate Change 2022: Impacts, Adaptation, and Vulnerability; Cambridge, UK and New York, USA, 2022.

(4) Gasser, T.; Kechiar, M.; Ciais, P.; Burke, E. J.; Kleinen, T.; Zhu, D.; Huang, Y.; Ekici, A.; Obersteiner, M. Path-dependent reductions in CO_2 emission budgets caused by permafrost carbon release. *Nat. Geosci.* **2018**, *11*(11), 830-835.

(5) Macdougall, A. H.; Zickfeld, K.; Knutti, R.; Matthews, H. D. Sensitivity of carbon budgets to permafrost carbon feedbacks and non-CO_2 forcings. *Environ. Res. Lett.* **2015**, *10*(12), 019501.

(6) Schaefer, K.; Hugues, L.; Vladimir, E. R.; Witt, E. A. G. S. The impact of the permafrost carbon feedback on global climate. *Environ. Res. Lett.* **2014**, *9*, 085003.

(7) Schuur, E. A. G.; Mcguire, A. D.; Schädel, C.; Grosse, G.; Harden, J. W.; Hayes, D. J.; Hugelius, G.; Koven, C. D.; Kuhry, P.; Lawrence, D. M.; Natali, S. M.; Olefeldt, D.; Romanovsky, V. E.; Schaefer, K.; Turetsky, M. R.; Treat, C. C.; Vonk, J. E. Climate change and the permafrost carbon feedback. *Nature* **2015**, *520*(7546), 171-179.

(8) Turetsky, M. R.; Abbott, B. W.; Jones, M. C.; Anthony, K. W.; Olefeldt, D.; Schuur, E. A. G.; Grosse, G.; Kuhry, P.; Hugelius, G.; Koven, C.; Lawrence, D. M.; Gibson, C.; Sannel, A. B. K.; Mcguire, A. D. Carbon release through abrupt permafrost thaw. *Nat. Geosci.* **2020**, *13*(2), 138-143.

(9) Chen, Y.; Romps, D. M.; Seeley, J. T.; Veraverbeke, S.; Riley, W. J.; Mekonnen, Z. A.; Randerson, J. T. Future increases in Arctic lightning and fire risk for permafrost carbon. *Nat. Clim. Chang.* **2021**, *11*(5), 404-410.

(10) Natali, S. M.; Holdren, J. P.; Rogers, B. M.; Treharne, R.; Duffy, P. B.; Pomerance, R.; Macdonald, E. Permafrost carbon feedbacks threaten global climate goals. *Proc. Natl. Acad. Sci. U. S. A.* **2021**, *118*(21), e2100163118.

(11) Natali, S. M.; Schuur, E. A. G.; Webb, E. E.; Pries, C. E. H.; Crummer, K. G. Permafrost degradation stimulates carbon loss from experimentally warmed tundra. *Ecology* **2014**, *95*(3), 602-608.

(12) Schaedel, C.; Koven, C. D.; Lawrence, D. M.; Celis, G.; Garnello, A. J.; Hutchings, J.; Mauritz, M.; Natali, S. M.; Pegoraro, E.; Rodenhizer, H.; Salmon, V. G.; Taylor, M. A.; Webb, E. E.; Wieder, W. R.; Schuur, E. A. G. Divergent patterns of experimental and model-derived permafrost ecosystem carbon dynamics in response to Arctic warming. *Environ. Res. Lett.* **2018**, *13*(10), 105002.

(13) Plaza, C.; Pegoraro, E.; Bracho, R.; Celis, G.; Crummer, K. G.; Hutchings, J. A.; Hicks Pries, C. E.; Mauritz, M.; Natali, S. M.; Salmon, V. G.; Schädel, C.; Webb, E. E.; Schuur, E. A. G. Direct observation of permafrost degradation and rapid soil carbon loss in tundra. *Nat. Geosci.* **2019**, *12*(8), 627-631.

(14) Olefeldt, D.; Goswami, S.; Grosse, G.; Hayes, D.; Hugelius, G.; Kuhry, P.; Mcguire, A. D.; Romanovsky, V. E.; Sannel, A. B. K.; Schuur, E. A. G.; Turetsky, M. R. Circumpolar distribution and carbon storage of thermokarst landscapes. *Nat. Commun.* **2016**, *7*, 13043.

(15) Miner, K. R.; Turetsky, M. R.; Malina, E.; Bartsch, A.; Tamminen, J.; Mcguire, A. D.; Fix, A.; Sweeney, C.; Elder, C. D.; Miller, C. E.; Anonymous. Permafrost carbon emissions in a changing Arctic. *Nat. Rev. Earth Environ.* **2022**, *3*(1), 55-67.

(16) Wauthy, M.; Rautio, M.; Christoffersen, K. S.; Forsström, L.; Laurion, I.; Mariash, H. L.; Peura, S.; Vincent, W. F. Increasing dominance of terrigenous organic matter in circumpolar freshwaters due to permafrost thaw. *Limnol. Oceanogr. Lett.* **2018**, *3*(3), 186-198.

(17) Bowen, J. C.; Ward, C. P.; Kling, G. W.; Cory, R. M. Arctic Amplification of Global Warming Strengthened by Sunlight Oxidation of Permafrost Carbon to CO_2. *Geophys. Res. Lett.* **2020**, *47*(12), e2020GL087085.

(18) Laurion, I.; Mladenov, N. Dissolved organic matter photolysis in Canadian arctic thaw ponds. *Environ. Res. Lett.* **2013**, *8*(3), 035026.

(19) Matveev, A.; Laurion, I.; Vincent, W. F. Methane and carbon dioxide emissions from thermokarst lakes on mineral soils. *Arct. Sci.* **2018**, *4*(4), 584-604.

(20) Ward, C. P.; Cory, R. M. Complete and Partial Photo-oxidation of Dissolved Organic Matter Draining Permafrost Soils. *Environ. Sci. Technol.* **2016**, *50*, 3545-3553.

(21) Ward, C. P.; Nalven, S. G.; Crump, B. C.; Kling, G. W.; Cory, R. M. Photochemical alteration of organic carbon draining permafrost soils shifts microbial metabolic pathways and stimulates respiration. *Nat. Commun.* **2017**, *8*, 772.

(22) Ward, C. P.; Cory, R. M. Assessing the prevalence, products, and pathways of dissolved organic matter partial photo-oxidation in arctic surface waters. *Environmental Science: Processes & Impacts* **2020**, *22*, 1214-1223.

(23) Delwiche, K. B.; Knox, S. H.; Malhotra, A.; Fluet-Chouinard, E.; Mcnicol, G.; Feron, S.; Ouyang, Z.; Papale, D.; Trotta, C.; Canfora, E.; Cheah, Y.; Christianson, D.; Alberto, M. C. R.; Alekseychik, P.; Aurela, M.; Baldocchi, D.; Bansal, S.; Billesbach, D. P.; Bohrer, G.; Bracho, R.; Buchmann, N.; Campbell, D. I.; Celis, G.; Chen, J.; Chen, W.; Chu, H.; Dalmagro, H. J.; Dengel, S.; Desai, A. R.; Detto, M.; Dolman, H.; Eichelmann, E.; Euskirchen, E.; Famulari, D.; Fuchs, K.; Goeckede, M.; Gogo, S.; Gondwe, M. J.; Goodrich, J. P.; Gottschalk, P.; Graham, S. L.; Heimann, M.; Helbig, M.; Helfter, C.; Hemes, K. S.; Hirano, T.; Hollinger, D.; Hörtnagl, L.; Iwata, H.; Jacotot, A.; Jurasinski, G.; Kang, M.; Kasak, K.; King, J.; Klatt, J.; Koebsch, F.; Krauss, K. W.; Lai, D. Y. F.; Lohila, A.; Mammarella, I.; Belelli Marchesini, L.; Manca, G.; Matthes, J. H.; Maximov, T.; Merbold, L.; Mitra, B.; Morin, T. H.; Nemitz, E.; Nilsson, M. B.; Niu, S.; Oechel, W. C.; Oikawa, P. Y.; Ono, K.; Peichl, M.; Peltola, O.; Reba, M. L.; Richardson, A. D.; Riley, W.; Runkle, B. R. K.; Ryu, Y.; Sachs, T.; Sakabe, A.; Sanchez, C. R.; Schuur, E. A.; Schäfer, K. V. R.; Sonnentag, O.; Sparks, J. P.; Stuart-Haëntjens, E.; Sturtevant, C.; Sullivan, R. C.; Szutu, D. J.; Thom, J. E.; Torn, M. S.; Tuittila, E.; Turner, J.; Ueyama, M.; Valach, A. C.; Vargas, R.; Varlagin, A.; Vazquez-Lule, A.; Verfaillie, J. G.; Vesala, T.; Vourlitis, G. L.; Ward, E. J.; Wille, C.; Wohlfahrt, G.; Wong, G. X.; Zhang, Z.; Zona, D.; Windham-Myers, L.; Poulter, B. and Jackson, R. B. FLUXNET-CH_4: a global, multi-ecosystem dataset and analysis of methane seasonality from freshwater wetlands. *Earth Syst. Sci. Data* **2021**, *13*(7), 3607-3689.

(24) Holgerson, M. A.; Raymond, P. A. Large contribution to inland water CO_2 and CH_4 emissions from very small ponds. *Nat. Geosci.* **2016**, *9*(3), 222-226.

(25) Virkkala, A.; Natali, S. M.; Rogers, B. M.; Watts, J. D.; Savage, K.; Connon, S. J.; Mauritz, M.; Schuur, E. A. G.; Peter, D.; Minions, C.; Nojeim, J.; Commane, R.; Emmerton, C. A.; Goeckede, M.; Helbig, M.; Holl, D.; Iwata, H.; Kobayashi, H.; Kolari, P.; López-Blanco, E.; Marushchak, M. E.; Mastepanov, M.; Merbold, L.; Parmentier, F. W.; Peichl, M.; Sachs, T.; Sonnentag, O.; Ueyama, M.; Voigt, C.; Aurela, M.; Boike, J.; Celis, G.; Chae, N.; Christensen, T. R.; Bret-Harte, M. S.; Dengel, S.; Dolman, H.; Edgar, C. W.; Elberling, B.; Euskirchen, E.; Grelle, A.; Hatakka, J.; Humphreys, E.; Järveoja, J.; Kotani, A.; Kutzbach, L.; Laurila, T.; Lohila, A.; Mammarella, I.; Matsuura, Y.; Meyer, G.; Nilsson, M. B.; Oberbauer, S. F.; Park, S.; Petrov, R.; Prokushkin, A. S.; Schulze, C.; St. Louis, V. L.; Tuittila, E.; Tuovinen, J.; Quinton, W.; Varlagin, A.; Zona, D. and Zyryanov, V. I. The ABCflux database: Arctic-boreal CO_2 flux observations and ancillary information aggregated to monthly time steps across terrestrial ecosystems. *Earth Syst. Sci. Data* **2022**, *14*(1), 179-208.

(26) Mazoyer, F.; Laurion, I.; Rautio, M. The dominant role of sunlight in degrading winter dissolved organic matter from a thermokarst lake in a subarctic peatland. *Biogeosciences* **2022**, *19*(17), 3959-3977.

(27) Liu, W.; Hegglin, M. I.; Checa-Garcia, R.; Li, S.; Gillett, N. P.; Lyu, K.; Zhang, X.; Swart, N. C. Stratospheric ozone depletion and tropospheric ozone increases drive Southern Ocean interior warming. *Nat. Clim. Chang.* **2022**, *12*(4), 365-372.

(28) Li, M.; Zhang, Q.; Zheng, B.; Tong, D.; Lei, Y.; Liu, F.; Hong, C.; Kang, S.; Yan, L.; Zhang, Y.; Bo, Y.; Su, H.; Cheng, Y.; He, K. Persistent growth of anthropogenic non-methane volatile organic compound (NMVOC) emissions in China during 1990 - 2017: drivers, speciation and ozone formation potential. *Atmos. Chem. Phys.* **2019**, *19*(13), 8897-8913.

(29) Hallquist, M.; Wenger, J. C.; Baltensperger, U.; Rudich, Y.; Simpson, D.; Claeys, M.; Dommen, J.; Donahue, N. M.; George, C.; Goldstein, A. H.; Hamilton, J. F.; Herrmann, H.; Hoffmann, T.; Iinuma, Y.; Jang, M.; Jenkin, M. E.; Jimenez, J. L.; Kiendler-Scharr, A.; Maenhaut, W.; Mcfiggans, G.; Mentel, T. F.; Monod, A.; Prevot, A. S. H.; Seinfeld, J. H.; Surratt, J. D.; Szmigielski, R.; Wildt, J. The formation, properties and impact of secondary organic aerosol: current and emerging issues. *Atmos. Chem. Phys.* **2009**, *9*, 5155-5236.

(30) Farmer, D. K.; Cappa, C. D.; Kreidenweis, S. M. Atmospheric Processes and Their Controlling Influence on Cloud Condensation Nuclei Activity. *Chem. Rev.* **2015**, *115*(10), 4199-4217.

(31) Moise, T.; Flores, J. M.; Rudich, Y. Optical Properties of Secondary Organic Aerosols and Their Changes by Chemical Processes. *Chem. Rev.* **2015**, *115*(10), 4400-4439.

(32) Gagnon, M.; Domine, F.; Boudreau, S. The carbon sink due to shrub growth on Arctic tundra: a case study in a carbon-poor soil in eastern Canada. *Environ. Res. Commun.* **2019**, *1*, 091001.

(33) Coulombe, O.; Bouchard, F.; Pienitz, R. Coupling of sedimentological and limnological dynamics in subarctic thermokarst ponds in Northern Québec (Canada) on an interannual basis. *Sediment. Geol.* **2016**, *340*, 15-24.

(34) Fewster, R. E.; Morris, P. J.; Ivanovic, R. F.; Swindles, G. T.; Peregon, A. M.; Smith, C. J. Imminent loss of climate space for permafrost peatlands in Europe and Western Siberia. *Nat. Clim. Chang.* **2022**, *12*(4), 373-379.

(35) Wang, X.; Dalton, E. Z.; Payne, Z. C.; Perrier, S.; Riva, M.; Raff, J. D.; George, C. Superoxide and Nitrous Acid Production from Nitrate Photolysis Is Enhanced by Dissolved Aliphatic Organic Matter. *Environ. Sci. Technol. Lett.* **2021**, *8*(1), 53-58.

(36) Wang, X.; Zhou, Y.; Li, K.; Pu, W.; Wang, X.; George, C. Snowmelt Leads to Seasonal Nitrous Acid Formation Across Northwestern China. *Geophys. Res. Lett.* **2022**, *49*(18), e2022GL098035.

(37) Lackner, G.; Domine, F.; Sarrazin, D.; Nadeau, D.; Belke-Brea, M. Hydrometeorological, snow and soil data from a low-Arctic valley in the forest-tundra ecotone in Northern Quebec, *PANGAEA* **2022**, DOI: 10.1594/PANGAEA.946538.

(38) Bernard, F.; Ciuraru, R.; Boréave, A.; George, C. Photosensitized Formation of Secondary Organic Aerosols above the Air/Water Interface. *Environ. Sci. Technol.* **2016**, *50*(16), 8678-8686.

(39) Rossignol, S.; Tinel, L.; Bianco, A.; Passananti, M.; Brigante, M.; Donaldson, J.; George, C. Atmospheric photochemistry at a fatty acid-coated air-water interface. *Science* **2016**, *353*(6300), 694-699.

(40) Abis, L.; Kalalian, C.; Lunardelli, B.; Wang, T.; Zhang, L.; Chen, J.; Perrier, S.; Loubet, B.; Ciuraru, R.; George, C. Measurement report: Biogenic volatile organic compound emission profiles of rapeseed leaf litter and its secondary organic aerosol formation potential. *Atmos. Chem. Phys.* **2021**, *21*(16), 12613-12629.

(41) Ciuraru, R.; Fine, L.; Pinxteren, M. V.; D Anna, B.; Herrmann, H.; George, C. Unravelling New Processes at Interfaces: Photochemical Isoprene Production at the Sea Surface. *Environ. Sci. Technol.* **2015**, *49*(22), 13199-13205.

(42) Ciuraru, R.; Fine, L.; van Pinxteren, M.; D Anna, B.; Herrmann, H.; George, C. Photosensitized production of functionalized and unsaturated organic compounds at the air-sea interface. *Sci. Rep.* **2015**, *5*(1), 12741.

(43) Brüggemann, M.; Hayeck, N.; George, C. Interfacial photochemistry at the ocean surface is a global source of organic vapors and aerosols. *Nat. Commun.* **2018**, *9*(1), 2101.

(44) Seinfeld, J. H.; Pandis, S. N., Atmospheric Chemistry and Physics, From Air Pollution to Climate Change; Wiley, New Jersey, USA, 2016.

(45) Müller, M.; Mikoviny, T.; Feil, S.; Haidacher, S.; Hanel, G.; Hartungen, E.; Jordan, A.; Märk, L.; Mutschlechner, P.; Schottkowsky, R.; Sulzer, P.; Crawford, J. H.; Wisthaler, A. A compact PTR-ToF-MS instrument for airborne measurements of volatile organic compounds at high spatiotemporal resolution. *Atmos. Meas. Tech.* **2014**, *7*(11), 3763-3772.

(46) Cappellin, L.; Biasioli, F.; Granitto, P. M.; Schuhfried, E.; Soukoulis, C.; Costa, F.; Märk, T. D.; Gasperi, F. On data analysis in PTR-TOF-MS: From raw spectra to data mining. *Sensors and Actuators B: Chemical* **2011**, *155*(1), 183-190.

(47) Xu, W.; Gao, Q.; He, C.; Shi, Q.; Hou, Z.; Zhao, H. Using ESI FT-ICR MS to Characterize Dissolved Organic Matter in Salt Lakes with Different Salinity. *Environ. Sci. Technol.* **2020**, *54*(20), 12929-12937.

(48) Bahureksa, W.; Tfaily, M. M.; Boiteau, R. M.; Young, R. B.; Logan, M. N.; Mckenna, A. M.; Borch, T. Soil Organic Matter Characterization by Fourier Transform Ion Cyclotron Resonance Mass Spectrometry (FTICR MS): A

Critical Review of Sample Preparation, Analysis, and Data Interpretation. *Environ. Sci. Technol.* **2021**, *55*(14), 9637-9656.

(49) Fu, H.; Ciuraru, R.; Dupart, Y.; Passananti, M.; Tinel, L.; Rossignol, S.; Perrier, S.; Donaldson, D. J.; Chen, J.; George, C. Photosensitized Production of Atmospherically Reactive Organic Compounds at the Air/Aqueous Interface. *J. Am. Chem. Soc.* **2015**, *137*(26), 8348-8351.

(50) Tinel, L.; Rossignol, S.; Bianco, A.; Passananti, M.; Perrier, S.; Wang, X.; Brigante, M.; Donaldson, D. J.; George, C. Mechanistic Insights on the Photosensitized Chemistry of a Fatty Acid at the Air/Water Interface. *Environ. Sci. Technol.* **2016**, *50*(20), 11041-11048.

(51) Domine, F.; Barrere, M.; Sarrazin, D.; Morin, S.; Arnaud, L. Automatic monitoring of the effective thermal conductivity of snow in a low-Arctic shrub tundra. *The Cryosphere* **2015**, *9*(3), 1265-1276.

(52) Lackner, G.; Domine, F.; Sarrazin, D.; Nadeau, D.; Belke-Brea, M. Radiation data from a tundra vegetation zone in the low-Arctic Tasiapik valley in the forest-tundra ecotone in Northern Quebec, *PANGAEA* **2022**, DOI: 10.1594/PANGAEA.946450.

(53) Kramshøj, M.; Albers, C. N.; Holst, T.; Holzinger, R.; Elberling, B.; Rinnan, R. Biogenic volatile release from permafrost thaw is determined by the soil microbial sink. *Nat. Commun.* **2018**, *9*(1), 3412.

(54) Kramshøj, M.; Albers, C. N.; Svendsen, S. H.; Björkman, M. P.; Lindwall, F.; Björk, R. G.; Rinnan, R. Volatile emissions from thawing permafrost soils are influenced by meltwater drainage conditions. *Glob. Change Biol.* **2019**, *25*(5), 1704-1716.

(55) Li, H.; Valiranta, M.; Maki, M.; Kohl, L.; Sannel, A. B. K.; Pumpanen, J.; Koskinen, M.; Back, J.; Bianchi, F. Overlooked organic vapor emissions from thawing Arctic permafrost. *Environ. Res. Lett.* **2020**, *15*(10), 104097.

(56) Anglada, J. M.; Martins-Costa, M. T. C.; Francisco, J. S.; Ruiz-López, M. F. Photoinduced Oxidation Reactions at the Air-Water Interface. *J. Am. Chem. Soc.* **2020**, *142*(38), 16140-16155.

(57) Cory; Ward, C. P.; Crump, B. C.; Kling, G. W. Sunlight controls water column processing of carbon in arctic fresh waters. *Science* **2014**, *345*(6199), 925-8.

(58) Perez, E. H.; Schleif, T.; Messinger, J. P.; Rullán Buxó, A. G.; Moss, O. C.; Greis, K.; Johnson, M. A. Structures and Chemical Rearrangements of Benzoate Derivatives Following Gas Phase Decarboxylation. *J. Am. Soc. Mass Spectrom.* **2022**, *33*(10), 1914-1920.

(59) Koch, B. P.; Dittmar, T. From mass to structure: an aromaticity index for high-resolution mass data of natural organic matter. *Rapid. Commun. Mass. Spectrom.* **2006**, *20*(5), 926-932.

(60) Chen, S.; Xie, Q.; Su, S.; Wu, L.; Zhong, S.; Zhang, Z.; Ma, C.; Qi, Y.; Hu, W.; Deng, J.; Ren, L.; Zhu, D.; Guo, Q.; Liu, C.; Jang, K.; Fu, P. Source and formation process impact the chemodiversity of rainwater dissolved organic matter along the Yangtze River Basin in summer. *Water Res.* **2022**, *211*, 118024.

(61) Heath, A. A.; Valsaraj, K. T. Effects of Temperature, Oxygen Level, Ionic Strength, and pH on the Reaction of Benzene with Hydroxyl Radicals at the Air–Water Interface in Comparison to the Bulk Aqueous Phase. *The Journal of Physical Chemistry A* **2015**, *119*(31), 8527-8536.

(62) Leng, C.; Kish, J. D.; Roberts, J. E.; Dwebi, I.; Chon, N.; Liu, Y. Temperature-Dependent Henry's Law Constants of Atmospheric Amines. *The Journal of Physical Chemistry A* **2015**, *119*(33), 8884-8891.

(63) Jones, B. M.; Grosse, G.; Arp, C. D.; Jones, M. C.; Walter Anthony, K. M.; Romanovsky, V. E. Modern thermokarst lake dynamics in the continuous permafrost zone, northern Seward Peninsula, Alaska. *Journal of Geophysical Research* **2011**, *116*, G00M03.

(64) Magnússon, R. Í.; Hamm, A.; Karsanaev, S. V.; Limpens, J.; Kleijn, D.; Frampton, A.; Maximov, T. C.; Heijmans, M. M. P. D. Extremely wet summer events enhance permafrost thaw for multiple years in Siberian tundra. *Nat. Commun.* **2022**, *13*, 1556.

(65) Vonk, J. E.; Tank, S. E.; Bowden, W. B.; Laurion, I.; Vincent, W. F.; Alekseychik, P.; Amyot, M.; Billet, M. F.; Canário, J.; Cory, R. M.; Deshpande, B. N.; Helbig, M.; Jammet, M.; Karlsson, J.; Larouche, J.; Macmillan, G.; Rautio, M.; Walter Anthony, K. M.; Wickland, K. P. Reviews and syntheses: Effects of permafrost thaw on Arctic aquatic ecosystems. *Biogeosciences* **2015**, *12*(23), 7129-7167.

(66) Bernard, F.; Ciuraru, R.; Boréave, A.; George, C. Photosensitized Formation of Secondary Organic Aerosols above the Air/Water Interface. *Environ. Sci. Technol.* **2016**, *50*(16), 8678-8686.

(67) Seco, R.; Holst, T.; Matzen, M. S.; Westergaard-Nielsen, A.; Li, T.; Simin, T.; Jansen, J.; Crill, P.; Friborg, T.; Rinne, J.; Rinnan, R. Volatile organic compound fluxes in a subarctic peatland and lake. *Atmos. Chem. Phys.* **2020**, *20*(21), 13399-13416.

(68) Matveev, A.; Laurion, I.; Deshpande, B. N.; Bhiry, N.; Vincent, W. F. High methane emissions from thermokarst lakes in subarctic peatlands. *Limnol. Oceanogr.* **2016**, *61*(S1), S150-S164.